May 6, 2008; revised June 30, 2008 FERMILAB-Pub-08-49-T

Quark and lepton masses from top loops

Bogdan A. Dobrescu and Patrick J. Fox

Theoretical Physics Department, Fermilab, Batavia, IL 60510, USA

Abstract

Assuming that the leptons and quarks other than top are massless at tree level, we show that their masses may be induced by loops involving the top quark. As a result, the generic features of the fermion mass spectrum arise from combinations of loop factors. Explicitly, we construct a renormalizable model involving a few new particles, which leads to 1-loop bottom and tau masses, a 2-loop charm mass, 3-loop muon and strange masses, and 4-loop masses for first generation fermions. This realistic pattern of masses does not require any symmetry to differentiate the three generations of fermions. The new particles may produce observable effects in future experiments searching for $\mu \to e$ conversion in nuclei, rare meson decays, and other processes.

1 Introduction

The masses of the six quarks and three charged leptons follow some intriguing patterns. At first sight, how heavy a fermion is depends crucially on which generation it belongs to. Fermions of the first generation are lighter by roughly two orders of magnitude than the corresponding fermions from the second generation, which in turn are two orders of magnitude lighter than the corresponding fermions from the third generation [1].

This pattern has motivated the study of models where the couplings of the fermions to the electroweak symmetry breaking sector are linear in the standard model fermion fields, so that the dominant contributions to the fermion mass matrices have rank one (*i.e.*, only the third generation fermions have large masses). The masses for the second generation are then induced at 1 loop [2] while first generation masses are further suppressed (attempts at deriving the electron mass from a loop involving the muon have a long history [3]).

In an interesting scheme of this type [4], a pair of vectorlike fermions mix with the standard model quarks such that only the top and bottom quarks have tree-level masses. A charge $-1/3$ scalar then couples the third generation quarks to the other quarks, resulting

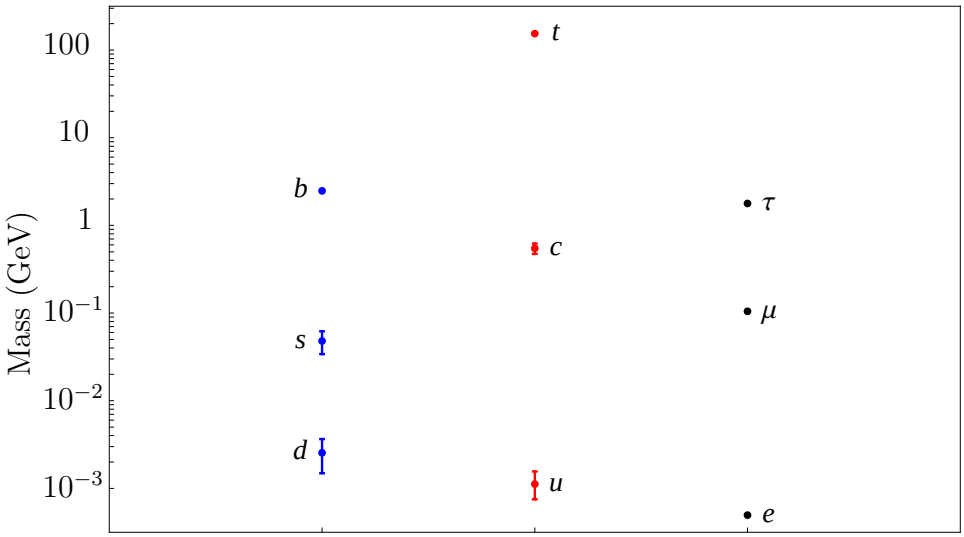

Figure 1: Quark and lepton masses at the 1 TeV scale, from Ref. [7].

in rank-two mass matrices at 1 loop and rank-three mass matrices at 2 loops. A similar scheme could be responsible for the lepton masses [5, 6], although the current constraints on neutrino masses push the mass of the new particles introduced in [5] above 10^{14} GeV, while the constraints on lepton flavor violating processes in the model of [6] render the muon and electron masses too small.

However, the fermion masses follow more complicated patterns, as displayed in Figure 1. Within the third generation, the b quark and the τ lepton are almost two orders of magnitude lighter than the top quark. The charm quark, which belongs to the second generation, is only a few times lighter than the b and τ. The other second generation fermions, namely the strange quark and the muon, are lighter by an additional order of magnitude.

Here we propose a mechanism for generating quark and lepton masses based on the assumption that only the top quark mass arises at tree level. In order to generate all the fermion masses, some new fields must couple the top quark to other standard model fermions. One might expect that such a mechanism would require a large number of fields, and furthermore that all the masses would arise at one loop. Remarkably, both these expectations turn out to be wrong due to the interplay of rank-one contributions to the mass matrices.

Concretely, we first introduce one scalar field that couples the top quark to the leptons (Section 2). This leads to masses for the τ, μ and the electron at 1, 3 and 5 loops

respectively. At the same time the charm and up quarks get masses at 2 and 4 loops respectively. In Section 3 we demonstrate that the top quark may be the only standard model fermion that acquires mass at tree level even when there is no new quantum number that differentiates it from the other quarks[1].

In order to generate the remaining quark masses we introduce (Section 4) some additional fields that couple to the down-type quarks, resulting in b, s and d masses at 1, 3 and 4 loops respectively. It turns out that these fields also contribute to the charm and up quark masses, and more importantly generate an electron mass at 4 loops. It is remarkable that this realistic pattern of loop-induced masses arises without need for any flavor symmetry to differentiate the three generations[2]. Furthermore, we show that the ensuing CKM matrix has elements consistent with experiment.

Various phenomenological constraints, discussed in Section 5, require the masses of some of the new particles to be substantially heavier than the electroweak scale. We envision that the gauge hierarchy problem is solved by supersymmetry or Higgs compositeness at the TeV scale. Although we do not explicitly embed our mechanism for fermion mass generation in a more complete theory of that type, we do not expect that such an embedding would encounter major hurdles. Note in particular that composite Higgs models based on top condensation [10, 11, 12] lead automatically to a large top mass, providing the appropriate input for the mechanism presented here.

The possibility that the mass of the top quark may be responsible for all other fermion masses has been previously considered [13, 14, 15]. Various obstacles [15], however, have prevented theories of this type from being realistic. In the model of Ref. [13] a weak-triplet VEV is essential for generating the lepton and first generation quark masses, such that the current constraints lead to an additional suppression of several orders of magnitude for all these masses. In the model of Ref. [14], if the mechanism is correctly continued all the way to the first generation, then the down quark turns out to be lighter than the up quark.

Our conclusions are collected in Section 6. In the Appendix we compute the 2-loop diagrams responsible for the charm mass.

---

[1] Alternatively, the top quark may be the only fermion with a tree-level mass because of some symmetry acting on the standard model fermions. A related model, where an S_3 symmetry allows tree-level masses only for the top and bottom quarks, is given in Ref. [9].

[2] Other models of fermion mass generation without flavor symmetries can be found, for example, in Refs. [8, 4].

2 Loop-induced masses for charged leptons and up-type quarks

We assume that the electroweak symmetry is spontaneously broken by the vacuum expectation value of a Higgs doublet H, and that the only nonzero Yukawa coupling of H to the standard model fermions is

$$- y_t \, \overline{u}_R^3 Q_L^3 \, H + \text{H.c.} \tag{2.1}$$

Here Q_L^i is the quark doublet of the ith generation, u_R^j is the up-type quark singlet of the jth generation, and y_t is a dimensionless parameter. The above Yukawa coupling breaks explicitly the $[U(3)]^3$ global symmetry of the quark kinetic terms down to a $U(1)_t \times U(2)_Q \times U(2)_u \times U(3)_d$ chiral symmetry, corresponding to unitary transformations acting on Q_L^3, $Q_L^{1,2}$, $u_R^{1,2}$ and the down-type quark singlets d_R^j, respectively. The top quark mass is generated at tree level ($m_t = y_t v_H > 0$, where $v_H \approx 174$ GeV), while the other quarks and leptons remain massless so far.

Let us introduce a complex scalar field, r, which transforms under $SU(3)_c \times SU(2)_W \times U(1)_Y$ as $(3,\, 2,\, +7/6)$. The normalization of hypercharge used here is $Y = Q - T^3$, where Q is the electric charge and T^3 is the diagonal $SU(2)_W$ generator. The r component of $T^3 = -1/2$ ($T^3 = +1/2$) has electric charge $+2/3$ ($+5/3$). The most general renormalizable interactions of r with standard model fermions are given by

$$\lambda_{ij} \, r \, \overline{u}_R^i L_L^j - \lambda'_{ij} \, r \, \overline{Q}_L^i e_R^j + \text{H.c.} \, , \tag{2.2}$$

where $i, j = 1, 2, 3$ label the generations, L_L^j are the lepton doublets, and e_R^j are the $SU(2)_W$-singlet electrically-charged leptons. The λ_{ij} and λ'_{ij} coefficients are dimensionless complex parameters.

The interactions (2.2) break explicitly the quark chiral symmetry down to $U(1)_u \times U(3)_d$, and the lepton chiral symmetry $U(3)_L \times U(3)_e$ down to $U(1)_L$. Here the $U(1)_u$ charge is an overall phase of the Q_L^i and u_R^i fields, while $U(1)_L$ charge is the lepton number. The conservation of these global charges implies that r carries baryon number $+1/3$ (same as Q_L^j) and lepton number $+1$ (same as L_L^j), so that it is a leptoquark.

The breaking of the chiral symmetries for the Q_L, u_R, L_L and e_R fields signals that all up-type quarks and electrically-charged leptons get masses at some loop level. Before computing the radiatively-induced masses, it is convenient to write the couplings (2.2) in a basis where there are as many zeroes as possible. The most general form of λ up to a

$U(2)_u \times U(3)_L$ transformation is

$$\lambda = \begin{pmatrix} \lambda_{11} & \lambda_{12} & 0 \\ 0 & \lambda_{22} & \lambda_{23} \\ 0 & 0 & \lambda_{33} \end{pmatrix} \ , \tag{2.3}$$

where all λ_{ij} are real and positive. Similarly, using the $U(2)_Q \times U(3)_e$ transformations, we can write

$$\lambda' = \begin{pmatrix} \lambda'_{11} & \lambda'_{12} & 0 \\ 0 & \lambda'_{22} & \lambda'_{23} \\ 0 & 0 & \lambda'_{33} \end{pmatrix} \ , \tag{2.4}$$

with $\lambda'_{ij} > 0$.

Let us now identify the leading loop diagrams that communicate electroweak symmetry breaking from the top quark to the leptons and the charm quark. The τ mass is induced at 1 loop, as shown in Figure 2, and is given by

$$m_\tau \simeq \lambda_{33}\lambda'_{33}\, m_t\, \epsilon_r^{(1)} \ , \tag{2.5}$$

where $\epsilon_r^{(1)}$ is the loop factor, which is logarithmically divergent:

$$\epsilon_r^{(1)} \simeq \frac{N_c}{16\pi^2} \ln\left(\frac{\Lambda^2}{M_r^2}\right) \ . \tag{2.6}$$

Here $N_c = 3$ is the number of colors, M_r is the mass of r, and Λ is the cutoff scale where the quark (other than top) and lepton masses vanish. For a cutoff $\Lambda \approx 10 M_r$ the loop factor is $\epsilon_r^{(1)} \approx 0.087$, and using the m_τ/m_t ratio at 1 TeV (see Figure 1) we find $\lambda_{33}\lambda'_{33} \approx (0.36)^2$. In Section 3 we will present a simple renormalizable model where the cutoff Λ is replaced by the mass of a new particle.

The charm quark mass is induced at two loops, through the "rainbow" diagram shown in Figure 3. The entries in the up-type quark mass matrix from this type of diagrams are given by

$$M_u[rr] = \begin{pmatrix} 0 & 0 & 0 \\ 0 & \lambda'_{23}\lambda_{23} & \lambda'_{33}\lambda_{23} \\ 0 & \lambda'_{23}\lambda_{33} & \lambda'_{33}\lambda_{33} \end{pmatrix} \lambda'_{33}\lambda_{33}\, m_t\, \epsilon_r^{(2)} \ , \tag{2.7}$$

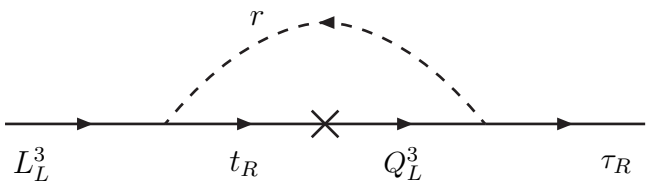

Figure 2: The 1-loop diagram responsible for the tau mass. The $\times$ represents a top quark mass insertion.

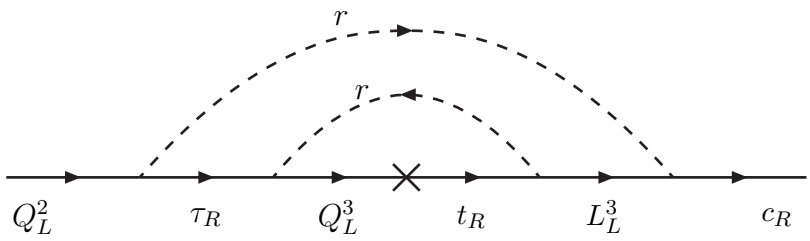

Figure 3: Charm mass induced by the 2-loop "rainbow" diagram involving the r scalar.

where $\epsilon_r^{(2)}$ is the 2-loop integral, and the corresponding term in the Lagrangian is $\overline{q}_R M_u q_L$. Approximating the inner loop in Figure 3 by Eq. (2.6), we find

$$\epsilon_r^{(2)} \simeq \frac{1}{N_c} \left(\epsilon_r^{(1)}\right)^2 \ . \tag{2.8}$$

In Appendix A we show that this is a reasonable approximation.

In addition to the "rainbow" diagram there are a few other 2-loop diagrams that connect a $Q_L^{2,3}$ external line to a c_R or t_R external line. These involve kinetic mixing between up-type quarks, and one can show that they do not change the rank of the up-type mass matrix. As a result, they may be ignored in the computation of the charm mass.

Given that the tree-level top mass represents a large contribution to the 33 element of the up-type quark mass matrix, the charm mass is approximately given by the 22 element of $M_u[rr]$:

$$m_c \simeq \lambda'_{23}\lambda_{23}\, m_\tau \, \frac{\epsilon_r^{(1)}}{N_c} \ . \tag{2.9}$$

Assuming that there are no other contributions to the charm mass, the m_c/m_τ ratio at 1 TeV requires $\lambda_{23}\lambda'_{23} \approx (3.3)^2$ for $\Lambda \approx 10 M_r$. These Yukawa couplings are rather large, and one may worry that they do not remain perturbative up to the scale Λ. However, in Section 4 it is shown that the sector responsible for the down-type quark masses actually leads to additional 2-loop contributions to m_c, so that the Yukawa couplings, λ_{23} and λ'_{23}, need not be that large.

Now that the charm quark has a mass, it will generate masses for the muon and up quark in the same way that the top mass lead to tau and charm masses. More precisely, the leading contributions to the muon mass arise from 3-loops diagrams involving one top-mass insertion. There are only two nonzero diagrams: a rainbow and a nonplanar diagram, shown in Figure 4. As in the case of the charm mass, diagrams involving kinetic

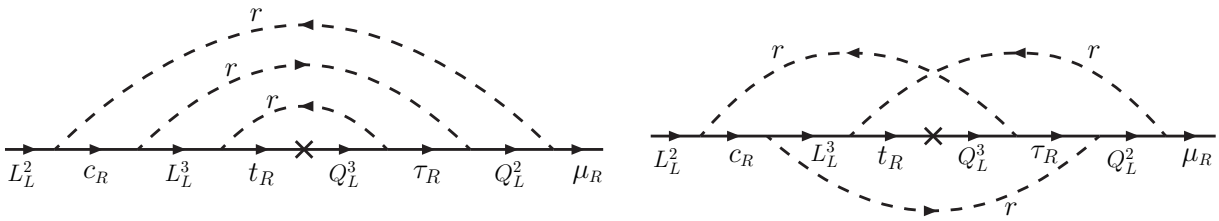

Figure 4: Muon mass induced by the 3-loop rainbow and nonplanar diagrams involving the r scalar. In the nonplanar diagram there is no intersection of the upper two r lines.

mixing on internal or external fermion lines may be ignored because they do not change the rank of the matrix (a more transparent argument is given in Section 3). The charged-lepton mass matrix gets the following contributions from diagrams involving three r lines:

$$M_e[rrr] = \begin{pmatrix} 0 & 0 & 0 \\ 0 & \lambda'_{22}\lambda'_{23}\lambda_{23}\lambda_{22} & \lambda'_{22}\lambda'_{23}\left[(\lambda_{23})^2+(\lambda_{33})^2\right] \\ 0 & \left[(\lambda'_{23})^2+(\lambda'_{33})^2\right]\lambda_{23}\lambda_{22} & \left[(\lambda'_{23})^2+(\lambda'_{33})^2\right]\left[(\lambda_{23})^2+(\lambda_{33})^2\right] \end{pmatrix} \lambda'_{33}\lambda_{33}\, m_t\, \epsilon_r^{(3)} \ . \tag{2.10}$$

In the large N_c limit the nonplanar diagram in Figure 4 is subleading to the rainbow diagram. In addition, the nonplanar diagram involves fewer factors of $\ln(\Lambda^2/M_r^2)$ (the 2-loop computations given in the Appendix include an explicit example of how fewer logarithmic factors arise in a non-rainbow diagram). Due to the combination of N_c and logarithmic factor suppression, we expect that the rainbow diagram dominates. So, the 3-loop factor, $\epsilon_r^{(3)}$, is given by

$$\epsilon_r^{(3)} \simeq \frac{1}{N_c}\left(\epsilon_r^{(1)}\right)^3 \ . \tag{2.11}$$

The 33 element of the charged-lepton mass matrix is dominated by the the 1-loop tau mass from Eq. (2.5), so that the muon mass is approximately given by the 22 element of $M_e[rrr]$:

$$m_\mu \simeq \lambda'_{22}\lambda_{22}\, m_c\, \epsilon_r^{(1)} \ . \tag{2.12}$$

The m_μ/m_c ratio at 1 TeV requires $\lambda_{22}\lambda'_{22} \approx (1.5)^2$.

The up-quark mass is generated at 4 loops. There are five diagrams, each involving four r lines. All these diagrams have 8 vertices, proportional to λ_{12}, λ_{22}, λ_{23}, λ_{33}, λ'_{33}, λ'_{32}, λ'_{22}, and λ'_{21}, respectively. The only difference between the diagrams comes from the way the four outgoing r lines are contracted with the four incoming r lines. If we label the above vertices by 1, 2, ... , 8, the pairing of r lines in the rainbow diagram is 18-27-36-45. In the large N_c limit, the rainbow diagram dominates, being of order N_c^2. However, there

are three other diagrams (18-25-36-47, 16-27-38-45, 14-27-36-58) of order N_c which cannot be neglected for $N_c = 3$. It is likely though that some of these diagrams have fewer factors of $\ln(\Lambda^2/M_r^2)$ than the rainbow diagram. The remaining diagram (16-25-38-47) does not depend on N_c. Thus, even though all these five diagrams have the same sign and add constructively, their sum may be reasonably well approximated by the rainbow diagram. The 4-loop contributions to the up-quark mass matrix take the form

$$M_u[rrrr]_{ij} = \left(\sum_{a,b,c,d} \lambda_{ia}\lambda_{ba}\lambda_{b3}\lambda'_{c3}\lambda'_{cd}\lambda'_{jd} \right) \lambda_{33}\lambda'_{33}\, m_t\, \epsilon_r^{(4)} \ , \tag{2.13}$$

where the 4-loop factor is expected to be of order

$$\epsilon_r^{(4)} \sim \frac{1}{N_c^2} \left(\epsilon_r^{(1)}\right)^4 \ . \tag{2.14}$$

The up quark mass is given approximately by the 11 entry of $M_u[rrrr]$:

$$m_u \approx \lambda'_{12}\lambda_{12}\, m_\mu \frac{\epsilon_r^{(1)}}{N_c} \ . \tag{2.15}$$

In the absence of contributions to the up mass from a different sector (see Section 4), the m_u/m_μ ratio at 1 TeV requires $\lambda_{12}\lambda'_{12} \approx (0.6)^2$, where we ignored the order-one uncertainty introduced by Eq. (2.14).

Finally, the electron mass arises at 5 loops. There are two diagrams at order N_c^3, eight diagrams at order N_c^2 and eleven diagrams at order N_c, all involving five r lines. Ignoring the uncertainty associated with the sum of these diagrams, we estimate

$$m_e \sim \lambda'_{11}\lambda_{11}\, m_u O(\epsilon_r^{(1)}) \ . \tag{2.16}$$

The m_u/m_e ratio at 1 TeV requires $\lambda_{11}\lambda'_{11} \approx (2.3)^2$. As in the case of the u or μ mass, all the diagrams contributing to the electron mass have the same sign. In the hypothetical case where all the loop integrals for non-rainbow diagrams have the same size as the rainbow one, the estimate for $\lambda_{11}\lambda'_{11}$ is smaller by a factor of $\sim (2.4)^2$.

The constraints on various processes induced by leptoquark exchange set limits on M_r far above 1 TeV (see section 5), so that the renormalization group evolution changes the quark and lepton masses at the scale M_r compared to the values shown in Figure 1. The most notable effect is that the quark masses decrease faster than the lepton masses when the scale where they are evaluated increases [7]. We have not taken this effect into account in this paper, because the field content above the TeV scale is not uniquely determined.

In summary, if the only source of mass for the up-type quarks and charged leptons is loops involving r, then the observed fermion masses, which span almost six orders of magnitude, may be obtained with values for the Yukawa couplings of r ranging between 0.36 and 3.3. Furthermore, the observed mass ordering $m_t > m_\tau > m_c > m_\mu > m_u > m_e$ is correctly reproduced by the number of loops required for generating each of these masses. Figure 5 depicts schematically how the masses for these fermions are generated. It is interesting to compare this figure with the fermion mass spectrum shown in Figure 1, keeping in mind that the mass decreases exponentially as the number of loops increases linearly.

In generating lepton masses from the top quark mass, a field with the quantum numbers of a leptoquark is generically necessary. There is however an alternative to the leptoquark (r) included here: a scalar $\tilde{d}$ transforming as $(\overline{3}, 1, +1/3)$ under $SU(3)_c \times SU(2)_W \times U(1)_Y$. The $\tilde{d}$ leptoquark has the quantum numbers of a right-handed down-type squark (note that in supersymmetric models with R-parity violation the squarks may have leptoquark couplings). The most general gauge invariant Yukawa couplings to the

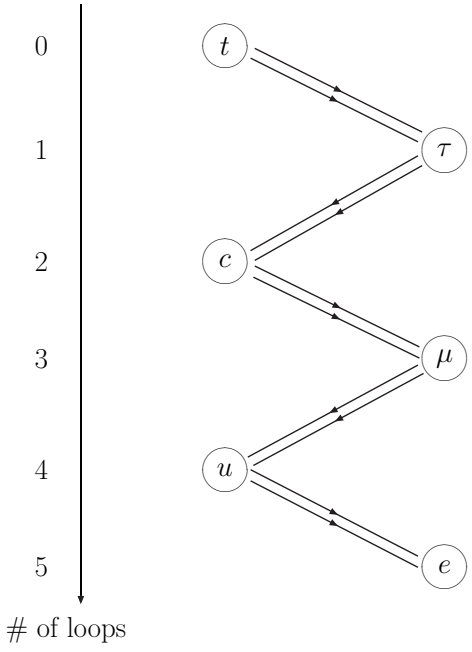

Figure 5: Loop-level where masses for charged leptons and up-type quarks are generated. Each line connecting a pair of fermions indicate Yukawa interactions with r.

standard model fermions are

$$\kappa_d \, \tilde{d} \, \overline{Q}_L^c \, L_L + \, \kappa'_d \, \tilde{d} \, \overline{u}_R^c \, e_R + \text{H.c.} \, , \tag{2.17}$$

where the flavor structure of the κ_d and κ'_d couplings is the same as in Eq. (2.3). The analysis carried out for r also applies to $\tilde{d}$: the above couplings break the chiral symmetries and lead to up-type quark and lepton masses, with the same loop counting. We will not discuss further the $\tilde{d}$ leptoquark in this paper.

3 Renormalizable UV completion

In the previous section we have assumed that the Higgs doublet couples only to the top quark at tree level. In this section we are going to justify this assumption by introducing a new symmetry acting on the Higgs sector (but not on the standard fermions) in a renormalizable model.

We introduce a symmetry, G_H, under which the Higgs doublet is charged while all standard model fermions are singlets. This forbids any dimension-4 couplings of the Higgs doublet to standard model fermions. The new symmetry is broken by the VEV of a scalar field ϕ which is a singlet under $SU(3)_c \times SU(2)_W \times U(1)_Y$. At this stage the chiral symmetries of the standard model are unbroken.

Examples of this symmetry could be a gauge or global $U(1)_H$, or a discrete subgroup thereof. We will consider, for concreteness, a global $U(1)_H$. As we will see, our minimal model would have to be extended if G_H is gauged since its fermion content is anomalous. For the case of a global $U(1)_H$ considered here this anomaly implies that the Goldstone boson has a small mass. However, this mass is not sufficient for $\langle \phi \rangle \lesssim 10^7$ TeV to avoid constraints from star cooling, and some additional small explicit breaking of $U(1)_H$ must be included to increase the mass of the would-be Goldstone boson. If G_H were discrete, then these constraints would be avoided, but instead one would need to ensure that the associated domain walls are cosmologically allowed. The solution to these problems should not affect the predictions we make here.

We introduce a vectorlike fermion, Ψ, transforming as Q_L under $SU(3)_c \times SU(2)_W \times U(1)_Y$, which carries $U(1)_H$ charge -1. Then the most general Yukawa couplings of ϕ and H are given by $H \overline{u}_R^i \Psi_L$ and $\phi \overline{\Psi}_R Q_L^j$. Without loss of generality we can use the chiral transformations to rewrite these Yukawa couplings as

$$- \, y_{\scriptscriptstyle H} H \, \overline{u}_R^3 \Psi_L - y_\phi \phi \, \overline{\Psi}_R Q_L^3 + \text{H.c.} \tag{3.1}$$

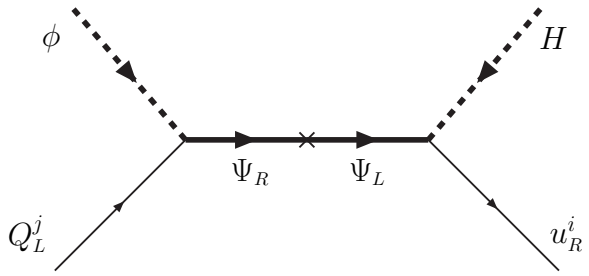

Figure 6: Top mass from an extended Higgs sector.

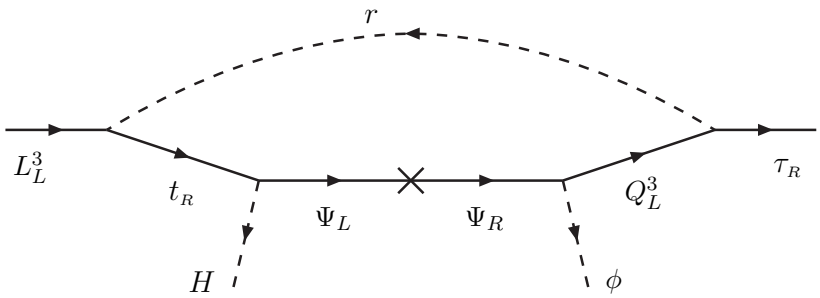

Figure 7: Effective operator responsible for the tau mass.

where y_H and y_ϕ are real positive parameters.

Integrating out the heavy Ψ fermion (see Figure 6) leads to a dimension-5 operator $\phi H\, \overline{u}_R^3\, Q_L^3$. Replacing the ϕ scalar by its VEV then leads to an effective top Yukawa coupling. The mass scale that suppresses this operator is given by the Ψ mass M_Ψ if $M_\Psi \gg y_\phi \langle\phi\rangle$. More generally, there is a 2×2 mass matrix for Ψ and top, whose lighest eigenvalue is the physical top mass. This is similar to the top-seesaw theory of Higgs compositeness [12]. For $y_H v_H \ll y_\phi \langle\phi\rangle$ and $y_H v_H \ll M_\Psi$,

$$m_t \approx y_H v_H \left[1 + \left(\frac{M_\Psi}{y_\phi \langle\phi\rangle}\right)^2\right]^{-1/2} . \tag{3.2}$$

A remarkable thing has happened: only the top quark acquires mass at tree level even when no symmetry differentiates it from other standard model fermions!

We can now repeat the analysis of Section 2 except instead of giving logarithmically divergent contributions to the fermion masses, the loops will generate *finite* coefficients to dimension-5 operators involving ϕ, H and a standard model fermion pair. For example, the coefficient of the $\phi H\, \overline{\tau}_R L_L^3$ operator arises from the 1-loop diagram shown in Figure 7,

and is given by $y_H y_\phi \lambda_{33}\lambda'_{33}\, N_c/M_\Psi$ times a finite integral:

$$\begin{aligned} I_1(M_\Psi, M_r) &= M_\Psi^2 \int \frac{d^4k}{(2\pi)^4}\, \frac{i}{k^2\,(k^2 - M_\Psi^2)\,(k^2 - M_r^2)} \\ &= \frac{1}{16\pi^2}\, \frac{M_\Psi^2}{M_\Psi^2 - M_r^2} \ln\left(\frac{M_\Psi^2}{M_r^2}\right) \ . \end{aligned} \tag{3.3}$$

Replacing H and ϕ by their VEVs, and using Eq. (3.2), we find the tau mass:

$$m_\tau \simeq \lambda_{33}\lambda'_{33}\, N_c m_t \left[1 + \left(\frac{y_\phi \langle\phi\rangle}{M_\Psi}\right)^2\right]^{1/2} I_1(M_\Psi, M_r) \ . \tag{3.4}$$

Comparing this result with Eq. (2.5) for $M_\Psi^2 \gg (y_\phi\langle\phi\rangle)^2$ and $M_\Psi \gg M_r$ shows that the cutoff scale used in Section 2 may be identified with the Ψ mass: $\Lambda \simeq M_\Psi$. For convenience we take this limit in what follows.

The UV completion discussed here results in only the top quark acquiring a tree-level coupling to the Higgs doublets, and implies that all the Yukawa couplings come from dimension-5 operators, of the form $\phi\, H\, \overline{\psi}_R\, \psi_L$. The lack of a renormalizable counterterm means that all fermion mass terms are finite. This justifies ignoring diagrams which involve kinetic mixing on internal or external lines, as we did earlier, because they contain fewer propagators in the loops and would lead to a mass with logarithmic dependence on the cutoff scale, which is forbidden by $U(1)_H$. Since kinetic mixing does not change the rank of the mass matrices, its presence in diagrams cannot lead to loop generated masses and it can be ignored.

4 Loop-induced down-type quark masses

With the fields and interactions introduced in the previous sections the chiral symmetry of the Lagrangian is $U(3)_d \times U(1)_u \times U(1)_L$. In order to generate masses for the b, s and d quarks, some new interactions must break the $U(3)_d$ symmetry by coupling the right-handed down-type quarks to fields involved in electroweak symmetry breaking. There are several possible interactions of this type. In this Section we focus for definiteness on a particular set of interactions.

4.1 b-quark mass

Let us introduce a pair of scalar fields, Φ_8 and Φ'_8, which transform under $SU(3)_c \times SU(2)_W \times U(1)_Y$ as $(8, 2, \pm 1/2)$, and carry global $U(1)_H$ charge $+1$. At the renormalizable

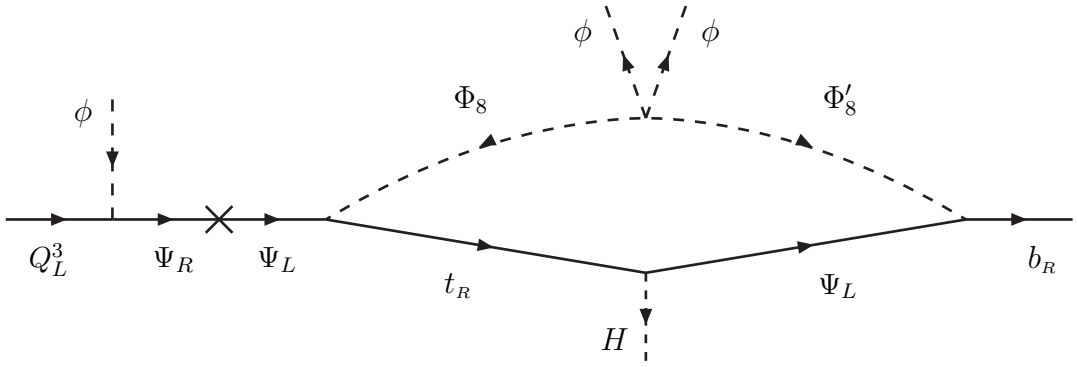

Figure 8: b-quark mass generated at one loop. The gauge-singlet scalar has a VEV $\langle\phi\rangle \sim M_\Psi$.

level, the most general couplings of Φ_8 and Φ'_8 to fermions are

$$\kappa_i \, \Phi_8 \, \overline{u}_R^i \Psi_L + \kappa' \, \Phi'_8 \, \overline{d}_R^3 \Psi_L + \text{H.c.} \; , \tag{4.1}$$

where κ_3 and κ' are positive parameters (up to a phase redefinition of Φ_8 and Φ'_8), while κ_1 and κ_2 are complex dimensionless parameters. Just as the Higgs doublet couples to only one linear combination of up-type quarks, Φ'_8 couples to only one linear combination of down-type quarks, which defines the bottom quark. The above interactions break explicitly the $U(3)_d \times U(1)_u$ chiral symmetry down to $U(2)_d$, so that they induce a mass for the b quark and not for the s and d quarks.

Besides the usual quartic couplings for the scalars, the

$$c \, \Phi_8 \Phi'_8 \phi\phi + c' \, H \Phi_8^\dagger r^\dagger r + c'' \left(\Phi_8 \, H^\dagger\right)^2 + \text{H.c.} \tag{4.2}$$

quartic couplings are allowed by all symmetries (the last coupling will not be used in the generation of fermion masses). The coefficients c' and c'' are complex numbers, while c is real and positive (its phase is absorbed by a redefinition of the Φ'_8 field, which in turn requires the same phase to be absorbed into d_R^3 in order to keep κ' real).

The b quark acquires a positive mass at one loop from the diagram shown in Figure 8:

$$m_b = \kappa_3 \kappa' c \, m_t \, \langle\phi\rangle^2 \, N_c \, \widetilde{I}_1(M_\Psi, M_8, M_{8'}) \; , \tag{4.3}$$

where M_8 and $M_{8'}$ are the masses of the Φ_8 and Φ'_8 scalars, and

$$\begin{aligned} \widetilde{I}_1(M_\Psi, M_8, M_{8'}) \;&\equiv\; \int \frac{d^4k}{(2\pi)^4} \, \frac{i}{(k^2 - M_\Psi^2)\,(k^2 - M_8^2)\,(k^2 - M_{8'}^2)} \\ &=\; \frac{M_{8'}^2 \, M_8^2 \ln\left(M_{8'}/M_8\right) + M_\Psi^2 \, M_{8'}^2 \ln\left(M_\Psi/M_{8'}\right) + M_8^2 \, M_\Psi^2 \ln\left(M_8/M_\Psi\right)}{8\pi^2 \left(M_{8'}^2 - M_8^2\right)\left(M_\Psi^2 - M_8^2\right)\left(M_\Psi^2 - M_{8'}^2\right)} \; . \end{aligned} \tag{4.4}$$

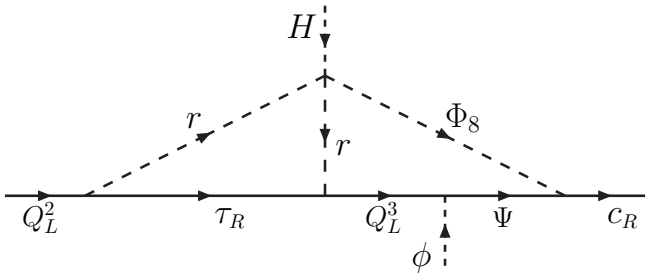

Figure 9: Charm-quark mass induced at 2 loops by the Φ_8 interactions.

Taking the limit $M_8 \ll M_\Psi,\ M_{8'}$, and to leading order in $(M_{8'}/M_\Psi)^2$, the integral of (4.4) becomes

$$\widetilde{I}_1(M_\Psi, M_8, M_{8'}) \approx \frac{1}{16\pi^2\, M_\Psi^2} \ln\left(\frac{M_\Psi^2}{M_8'^2}\right) \ . \tag{4.5}$$

As before, this mass is a finite effect with the logarithm being cutoff by the mass of the massive fermion. Working in this regime and assuming that $\langle\phi\rangle \approx M_\Psi$ and $y_\phi^2 \ll 1$ we find that the correct b-quark mass requires $\kappa_3\, \kappa' c \approx (0.6)^3$, for $M_\Psi/M_{8'} \sim O(10)$.

In addition to the masses generated in section 2 when r was integrated out, there are potentially important contributions to the charm, up and electron masses from the fields introduced in this section.

The charm-quark mass receives an additional two-loop contribution from the diagram shown in Figure 9. This is a direct contribution from the Higgs VEV, unlike the two-loop contribution to the charm mass discussed in Section 2, which first required the tau to get a mass. However, as before, this new contribution does involve a top-quark internal line. The new two-loop contributions to the mass matrix of the up-type quarks are given by

$$M_u[\Phi_8 r] = \begin{pmatrix} 0 & \kappa_1\lambda'_{23} & \kappa_1\lambda'_{33} \\ 0 & \kappa_2\lambda'_{23} & \kappa_2\lambda'_{33} \\ 0 & \kappa_3\lambda'_{23} & \kappa_3\lambda'_{33} \end{pmatrix} \lambda'_{33} c' \, \frac{y_\phi \, \langle\phi\rangle \, v_H}{M_\Psi} \, \epsilon_\Phi^{(2)} \ . \tag{4.6}$$

Here $\epsilon_\Phi^{(2)}$ is a 2-loop integral computed in the Appendix [see Eq. (A.4)], which is parametrically smaller than the $\epsilon_r^{(2)}$ integral of Eq.(2.8) by a logarithmic factor. Nevertheless, the above contribution to the charm mass is not suppressed by the small product of couplings $\lambda_{33}\lambda'_{33}$, and therefore it may be comparable to or even larger than the rainbow diagram of Figure 3. Consequently, λ_{23} and λ'_{23} may be substantially smaller than the values determined in Section 2.

The up-quark mass also gets additional contributions, at 4 loops, from diagrams that involve one $H\Phi_8^\dagger r^\dagger r$ vertex [see Eq. (4.2)] and either a $(r^\dagger r)^2$ or $\Phi_8^\dagger \Phi_8 r^\dagger r$ vertex. We will ignore these diagrams in what follows because they are probably suppressed by one

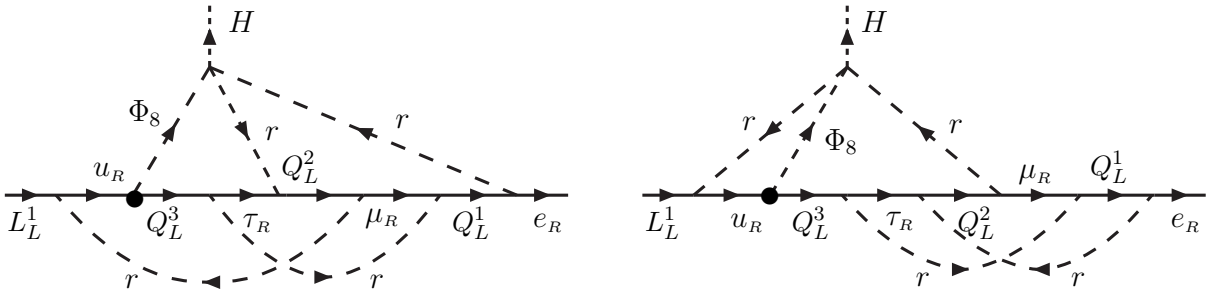

Figure 10: Electron mass induced at 4 loops. The diagrams are nonplanar (the lower two r lines do not intersect). The $\bullet$ indicates a vertex obtained by integrating out the Ψ fermion.

logarithmic factor compared with the 4-loop contributions discussed in Section 2. It should be mentioned, though, that it is difficult to determine the largest number of logarithmic factors appearing in such 4-loop integrals, especially because some of these are associated with infrared divergences for $M_r \to 0$.

Interestingly, the interactions of the Φ_8 lead to an electron mass induced at 4 loops, as shown in Figure 10. Recall that the r interactions by themselves allowed an electron mass only at 5 loops. It is thus likely that the 4-loop diagrams of Figure 10 represent the dominant contributions to the electron mass. Hence, the $\lambda_{11}\lambda'_{11}$ product may be smaller than the value derived from Eq. (2.16) without affecting the electron mass, which somewhat relaxes the limits on the r leptoquark (see Section 5). On the other hand, these 4-loop diagrams include fewer than four logarithmic factors, while the 5-loop contributions are enhanced by the large number of diagrams, so that without a detailed computation it cannot be ruled out that the two contributions are comparable for sizable ranges of parameters. Assuming that the diagrams in Figure 10 dominate and lead to three logarithmic factors (*i.e.*, one less than a 4-loop rainbow diagram, as suggested by the 2-loop computations presented in the Appendix), we find

$$m_e \approx \lambda_{11}\,\lambda'_{11}\,\lambda'_{12}\,\lambda'_{22}\,\lambda'_{23}\,\lambda'_{33}\,\kappa_1^*\,c'^*\,\frac{y_\phi\langle\phi\rangle}{M_\Psi}\,v_H\,\epsilon_\Phi^{(4)}\ , \tag{4.7}$$

where the 4-loop factor is

$$\epsilon_\Phi^{(4)} \sim \frac{N_c^2}{(16\pi^2)^4}\ln^3\left(\frac{M_\Psi^2}{M_r^2}\right)\ . \tag{4.8}$$

The m_e/v_H ratio is correctly reproduced for

$$\lambda_{11}\,\lambda'_{11}\,\lambda'_{12}\,\lambda'_{22}\,\lambda'_{23}\,\lambda'_{33}\,\kappa_1^*\,c'^*\ \sim 2\ . \tag{4.9}$$

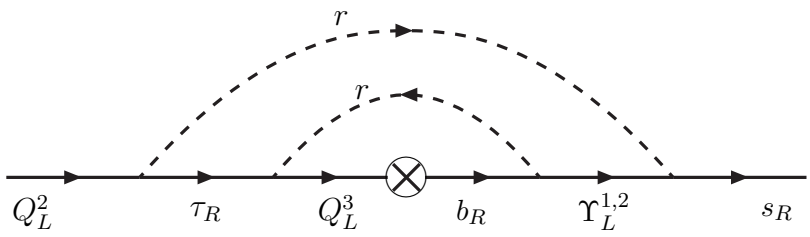

Figure 11: Strange mass induced by a 3-loop "rainbow" diagram. The $\otimes$ symbol represents the b mass induced at 1-loop as in Fig. 8.

4.2 Strange and down quark masses

The strange and down quarks remain massless until the $U(2)_d$ symmetry is broken. One possibility for breaking that chiral symmetry is to introduce some vectorlike fermions Υ^k which transform as $(1, 2, +3/2)$ under $SU(3)_c \times SU(2)_W \times U(1)_Y$. It is sufficient to include two such fermions: $k = 1, 2$. Their most general Yukawa interactions with the fields introduced here are

$$\eta_{jk}\, r\, \overline{d}_R^{\,j} \Upsilon^k + \text{H.c.} \tag{4.10}$$

An $U(2)_d$ transformation allows us to take $\eta_{11} = 0$. We may also redefine the phases of the s_R and d_R fields such that 3 combinations of η_{ij} parameters are real, but it is more convenient to do so after we compute the strange and down quark masses.

The strange-quark mass is generated at 3 loops by the diagram shown in Figure 11. The contributions to the down-type quark mass matrix from this type of 3-loop rainbow diagrams are approximately given by

$$M_d[rr\Phi_8] \approx \begin{pmatrix} 0 & 0 & 0 \\ 0 & (\eta_{21}\,\eta_{31}^* + \eta_{22}\,\eta_{32}^*)\,\lambda'_{23} & (\eta_{21}\,\eta_{31}^* + \eta_{22}\,\eta_{32}^*)\,\lambda'_{33} \\ 0 & \left(|\eta_{31}|^2 + |\eta_{32}|^2\right)\lambda'_{23} & \left(|\eta_{31}|^2 + |\eta_{32}|^2\right)\lambda'_{33} \end{pmatrix} \lambda'_{33}\, m_b\, \epsilon_r^{(2)} \ , \tag{4.11}$$

where $\epsilon_r^{(2)}$ is the dimensionless 2-loop integral for a rainbow diagram [see Eq.(2.8)]. We have assumed here that the vectorlike fermions $\Upsilon^{1,2}$ have negligible masses compared to M_r. Since there is a 1-loop contribution to the b-quark mass (the 33 element of M_d), the s-quark mass is approximately given by the 22 element of $M_d[rr\Phi_8]$. An s_R field redefinition allows us to make the $\eta_{21}\,\eta_{31}^* + \eta_{22}\,\eta_{32}^*$ combination real and positive, so that all entries in Eq. (4.11) are positive.

The $m_s/m_b \sim 1/50$ mass ratio requires a product of dimensionless couplings to be

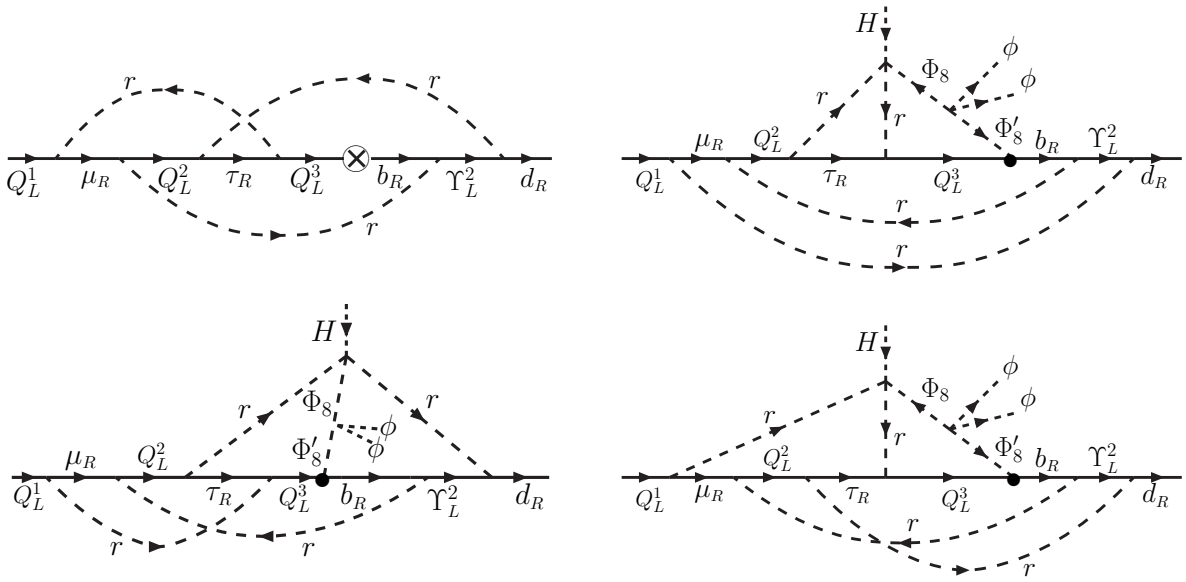

Figure 12: Down-quark mass induced at 4 loops. In the first diagram, the $\otimes$ represents the 1-loop b-mass insertion of Fig. 8, and the upper two r lines do not intersect. The last two diagrams are also nonplanar (the lower two r lines do not intersect). As before the $\bullet$ indicates a vertex obtained by integrating out the Ψ fermion.

larger than unity:

$$(\eta_{21}\,\eta_{31}^* + \eta_{22}\,\eta_{32}^*)\,\lambda'_{23}\lambda'_{33} \sim 8\ . \tag{4.12}$$

However, given that several couplings are involved here, none of them needs to be substantially larger than unity, and therefore we do not need to worry about departures from perturbativity.

The down-quark mass is generated at 4 loops through the diagrams shown in Figure 12, and is given by

$$m_d \approx \lambda'_{12}\,\lambda'_{22}\,\lambda'_{23}\,\lambda'_{33}\,\eta_{32}^*\,\eta_{12}\left[m_b\,\epsilon_\Upsilon^{(3)} + y_\phi\,v_H\kappa' c\,c'\left(\frac{\langle\phi\rangle}{M_\Psi}\right)^3\epsilon_\Upsilon^{(4)}\right]\ . \tag{4.13}$$

The first term in the paranthesis represents the first diagram in Figure 12, and involves a 3-loop nonplanar integral $\epsilon_\Upsilon^{(3)}$. The second term represents the sum of the last three diagrams, and involves a 4-loop dimensionless integral $\epsilon_\Upsilon^{(4)}$. Although we have not calculated $\epsilon_\Upsilon^{(3)}$ and $\epsilon_\Upsilon^{(4)}$, the second term is likely to dominate because it is enhanced by a factor of N_c^2: $\epsilon_\Upsilon^{(4)} \sim \epsilon_\Phi^{(4)}$, with $\epsilon_\Phi^{(4)}$ given in Eq. (4.8). Similar 4-loop diagrams contribute to all $1i$ and $i1$ ($i = 1, 2, 3$) entries of the down-type mass matrix.

Using a phase redefinition of d_R, we take $m_d > 0$ in Eq. (4.13). This implies $\eta_{32}^*\eta_{12}c' >$

	H	ϕ	$\Psi_{L,R}$	r	Φ_8	Φ'_8	$\Upsilon^{1,2}_{L,R}$
$SU(3)_c$	1	1	3	3	8	8	1
$SU(2)_W$	2	1	2	2	2	2	2
$U(1)_Y$	$+1/2$	0	$+1/6$	$+7/6$	$+1/2$	$-1/2$	$+3/2$
global $U(1)_H$	$+1$	-1	-1	0	$+1$	$+1$	0
spin	0	0	1/2	0	0	0	1/2

Table 1: Charges of scalars and vectorlike quarks. H breaks the electroweak symmetry, ϕ and Ψ communicate the breaking to the t quark, r communicates it to the charged leptons and the c and u quarks, while the fields on the right-hand side are responsible for down-type quark masses.

0, assuming that the first term is negligible. The interactions (4.10) and the phase redefinitons discussed in this section finally break the chiral symmetry $[U(3)]^5$ of the standard model fermions down to $U(1)_L \times U(1)_Q$, corresponding to lepton and quark number respectively.

The $m_d/v_H \approx 1.4 \times 10^{-5}$ ratio also requires a product of dimensionless couplings to be large:

$$\lambda'_{12}\,\lambda'_{22}\,\lambda'_{23}\,\lambda'_{33}\,\eta^*_{32}\,\eta_{12}\,y_\phi\,\kappa' c\,c' \sim O(10) \tag{4.14}$$

for $\langle\phi\rangle \approx M_\Psi$. As in the case of m_s, the large number of couplings allows the product to be large even if no coupling is substantially larger than unity.

To summarize the field content of our model, the masses of the up-type quarks and charged leptons are generated by the fields shown on the left-hand side of Table 1, while the masses of the down-type quarks also require the fields shown on the right-hand side of Table 1.The mechanism of fermion mass generation is schematically depicted in Figure 13.

4.3 CKM matrix

In the previous sections we have determined the leading piece of each entry in the mass matrix for both the up- and down-type quarks. The transformations necessary to go to the mass eigenstate basis will determine the CKM matrix. The mass terms for the quarks are $\overline{q}_R M_q q_L$ $(q = u, d)$. Working in the regime where the charm quark gets its mass

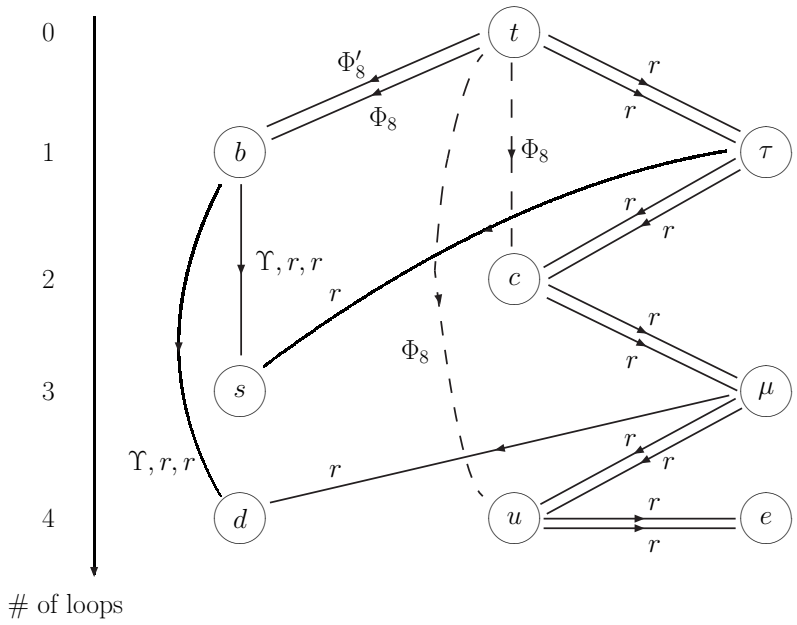

Figure 13: Loop-level of mass generation. Each line connecting a pair of fermions indicates interactions that break their chiral symmetries. A fermion receives a mass provided at least two lines connect it to other fermions which communicate with the Higgs sector (the chiral symmetries of both its left- and right-handed components must be broken).

predominantly from diagrams involving Φ_8, so that (4.6) dominates over (2.7), we find

$$M_u \approx \begin{pmatrix} m_u & \frac{\kappa_1}{\kappa_2}\, m_c & \frac{\kappa_1 \lambda'_{33}}{\kappa_2 \lambda'_{23}}\, m_c \\ a_u m_u & m_c & \frac{\lambda'_{33}}{\lambda'_{23}}\, m_c \\ \frac{\lambda_{33}}{\lambda_{23}}\left(a_u - \frac{\lambda_{22}}{\lambda_{12}}\right) m_u & \frac{\kappa_3}{\kappa_2}\, m_c & m_t \end{pmatrix} , \tag{4.15}$$

where we defined

$$a_u \equiv \frac{\lambda_{22}^2 + \lambda_{23}^2 + \lambda_{33}^2}{\lambda_{12}\lambda_{22}} > 0 \ . \tag{4.16}$$

The only complex entries in M_u are those involving κ_1 or κ_2. The down-type quark mass matrix is given by

$$M_d \approx \begin{pmatrix} m_d & \dfrac{\lambda'^2_{22}+\lambda'^2_{23}+\lambda'^2_{33}}{\lambda'_{12}\lambda'_{22}}\, m_d & \dfrac{\lambda'_{33}(\lambda'^2_{23}+\lambda'^2_{33})}{\lambda'_{12}\lambda'_{22}\lambda'_{23}}\, m_d \\ a_d\, m_d & m_s & \dfrac{\lambda'_{33}}{\lambda'_{23}}\, m_s \\ a_d\, a_s\, m_d & a_s\, m_s & m_b \end{pmatrix} , \tag{4.17}$$

where, for convenience we introduced the notation

$$a_d = \frac{\eta_{21}\,\eta^*_{31}+\eta_{22}\,\eta^*_{32}}{\eta_{12}\,\eta^*_{32}} ,$$

$$a_s = \frac{|\eta_{31}|^2+|\eta_{32}|^2}{\eta_{21}\,\eta^*_{31}+\eta_{22}\,\eta^*_{32}} > 0 . \tag{4.18}$$

Note that a_d is the only complex parameter, and the only complex entries in M_d are the 21 and 31 ones.

The CKM matrix is determined by the unitary transformations, V_{u_L} and V_{d_L}, of the left-handed quark fields that diagonalize the mass matrices (more precisely, the 3×3 matrices $V_{q_L} M_q^\dagger M_q V_{q_L}^\dagger$ for $q = u, d$ are diagonal). For the up-type quarks this transformation is

$$V_{u_L} \approx \begin{pmatrix} 1 & -\dfrac{\kappa_1/\kappa_2+a_u}{1+|\kappa_1/\kappa_2|^2}\,\dfrac{m_u}{m_c} & 0 \\ \dfrac{\kappa_1^*/\kappa_2^*+a_u}{1+|\kappa_1/\kappa_2|^2}\,\dfrac{m_u}{m_c} & 1 & -\dfrac{\kappa_3}{\kappa_2^*}\,\dfrac{m_c}{m_t} \\ 0 & \dfrac{\kappa_3}{\kappa_2}\,\dfrac{m_c}{m_t} & 1 \end{pmatrix} , \tag{4.19}$$

where we have ignored all quadratic corrections in m_u/m_c or m_c/m_t (these ratios are 2-loop factors, as shown in Figure 13). For the down-type quarks, we keep only linear terms in m_s/m_b (which is a 2-loop factor) but we keep the quadratic terms in m_d/m_s (which is a 1-loop factor):

$$V_{d_L} \approx \begin{pmatrix} 1-\dfrac{|a_d|^2}{2}\left(\dfrac{m_d}{m_s}\right)^2 & -a_d^*\dfrac{m_d}{m_s} & 0 \\ a_d\dfrac{m_d}{m_s} & 1-\dfrac{|a_d|^2}{2}\left(\dfrac{m_d}{m_s}\right)^2 & -a_s\,\dfrac{m_s}{m_b} \\ a_d\,a_s\,\dfrac{m_d}{m_b} & a_s\,\dfrac{m_s}{m_b} & 1 \end{pmatrix} \tag{4.20}$$

The CKM matrix is then given by

$$V_{u_L} V_{d_L}^\dagger \approx \begin{pmatrix} 1 - \frac{|a_d|^2}{2}\left(\frac{m_d}{m_s}\right)^2 & a_d^* \frac{m_d}{m_s} & a_d^* a_s \frac{m_d}{m_b} \\ -a_d \frac{m_d}{m_s} & 1 - \frac{|a_d|^2}{2}\left(\frac{m_d}{m_s}\right)^2 & a_s \frac{m_s}{m_b} - \frac{\kappa_3}{\kappa_2^*}\frac{m_c}{m_t} \\ -a_d \frac{\kappa_3}{\kappa_2}\frac{m_c m_d}{m_t m_s} & -a_s \frac{m_s}{m_b} + \frac{\kappa_3}{\kappa_2}\frac{m_c}{m_t} & 1 \end{pmatrix} . \tag{4.21}$$

All off-diagonal entries of this matrix are complex, but one may absorb four phases in the u_L^i and d_L^i fields, leaving complex phases only into the 13 and 31 entries. The result is the CKM matrix in the Wolfenstein parametrization [16],

$$V_{\rm CKM} \approx \begin{pmatrix} 1 - \frac{\lambda^2}{2} & \lambda & A\lambda^3 (\rho - i\eta) \\ -\lambda & 1 - \frac{\lambda^2}{2} & A\lambda^2 \\ A\lambda^3 (1 - \rho - i\eta) & -A\lambda^2 & 1 \end{pmatrix} , \tag{4.22}$$

with the Wolfenstein parameters given in terms of our combinations of couplings by

$$\begin{aligned} \lambda &= |a_d| \frac{m_d}{m_s} , \\ A &= \frac{1}{\lambda^2} \left| a_s \frac{m_s}{m_b} - \frac{\kappa_3}{\kappa_2^*}\frac{m_c}{m_t} \right| , \\ \rho &= \frac{a_s}{A^2\lambda^4}\frac{m_s}{m_b}\left[a_s \frac{m_s}{m_b} - {\rm Re}\left(\frac{\kappa_3}{\kappa_2}\right)\frac{m_c}{m_t} \right] , \\ \eta &= \frac{a_s}{A^2\lambda^4} {\rm Im}\left(\frac{\kappa_3}{\kappa_2}\right)\frac{m_s}{m_b}\frac{m_c}{m_t} , \end{aligned} \tag{4.23}$$

These equations can be inverted:

$$\begin{aligned} |a_d| &= \lambda \frac{m_s}{m_d} \approx 4.4 , \\ a_s &= A\lambda^2 \sqrt{\rho^2 + \eta^2}\, \frac{m_b}{m_s} \approx 0.84 , \\ \frac{\kappa_3}{\kappa_2} &= \frac{A\lambda^2}{\sqrt{\rho^2 + \eta^2}} \frac{m_t}{m_c} \left[\eta^2 + \rho^2 - \rho + i\eta \right] \approx -1.6 + 8.9\, i , \end{aligned} \tag{4.24}$$

where the numerical values used here are $\lambda \approx 0.227$, $A \approx 0.818$, $\rho \approx 0.22$, and $\eta \approx 0.34$ [1]. The ratios $|a_d|$ and $\mathrm{Im}(\kappa_3/\kappa_2)$ are larger than order one, but overall the CKM matrix elements are well reproduced in our model for reasonable values of parameters.

5 Experimental Constraints

The domino mechanism described above works at any scale provided there is some separation between the masses of the domino particles and the cutoff scale (set by the mass of the Ψ fermion). However, if the mass scales are low enough it may be possible to directly produce some of the new states or to probe them indirectly by their effects on rare processes. For instance, leptoquarks induce rare meson decays, rare μ and τ decays, $\mu \to e$ conversion in nuclei, meson anti-meson mixing and other processes [17]. The constraints from rare processes typically bound the ratios λ_{ij}/M_r or λ_{ij}^2/M_r. Since we know the approximate size of the couplings necessary to give the correct quark and lepton masses, we derive a lower bound on the leptoquark mass.

The conversion of $\mu \to e$ in nuclei can take place at tree level through exchange of the leptoquark. At low-energy, the relevant piece of the effective Lagrangian, after a Fierz transformation, is

$$\frac{1}{4M_r^2}\Big[\bar{u}u\,(\lambda'_{11}\lambda_{12}\,\bar{e}_R\mu_L + \lambda_{11}\lambda'_{12}\,\bar{e}_L\mu_R) - \bar{u}\gamma_\mu u\,(\lambda_{11}\lambda_{12}\,\bar{e}_L\gamma^\mu\mu_L + \lambda'_{11}\lambda'_{12}\,\bar{e}_R\gamma^\mu\mu_R) - \lambda'_{11}\lambda'_{12}\,\bar{d}\gamma_\mu d\,\bar{e}_R\gamma^\mu\mu_R\Big]\ . \tag{5.1}$$

The above terms involving u quarks arise from the exchange of the r component carrying weak isospin $+1/2$, while the terms involving d quarks arises from the one carrying weak isospin $-1/2$. Following Ref. [19], we find that the above four-fermion interactions give the following rate for coherent $\mu \to e$ conversion in nuclei:

$$\Gamma(\mu \to e) = \frac{m_\mu^5}{4M_r^4}\left\{\lambda_{11}^2\left[\lambda'_{12}S_0 - \lambda_{12}\left(2V^{(p)} + V^{(n)}\right)\right]^2 + \lambda_{11}'^2\left[\lambda_{12}S_0 - 3\lambda'_{12}\left(V^{(p)} + V^{(n)}\right)\right]^2\right\} \tag{5.2}$$

where $V^{(p)}$ ($V^{(n)}$) is the overlap integral of the proton (neutron) density and the electron and muon wavefunctions associated with vector operators, and S_0 is a combination of similar integrals for scalar operators. For Titanium, these are [19]: $V^{(p)} = 0.0396$, $V^{(n)} = 0.0468$ and $S_0 \approx 0.375$. The experimental limit on muon conversion [1] in Titanium is

$$\frac{\Gamma(\mu\,\mathrm{Ti} \to e\,\mathrm{Ti})}{\Gamma(\mu\,\mathrm{Ti} \to \mathrm{capture})} < 4.3 \times 10^{-12}. \tag{5.3}$$

Thus, we find a limit

$$M_r > 290\,\text{TeV}\left[\lambda_{11}^2\left(\lambda_{12}-3.0\lambda'_{12}\right)^2+\lambda'^2_{11}\left(3.0\lambda_{12}-2.1\lambda'_{12}\right)^2\right]^{1/4}\ . \tag{5.4}$$

The Yukawa couplings here are in the mass eigenstate basis, whereas the ones introduced in section 2 are given in the weak eigenstate basis. Given that the two bases are roughly aligned, we will not make the distinction explicit in what follows. The m_u/m_μ ratio requires $\lambda_{12}\lambda'_{12}\sim(0.6)^2$, as discussed in Section 2. Likewise, the product $\lambda_{11}\lambda'_{11}$ cannot be too small, or else the loop-generated electron mass will not be consistent with the measured value. Nevertheless, several of the couplings in Eq. (4.9) may be larger than unity, allowing $\lambda_{11}\lambda'_{11}\sim 0.1$. For $\lambda_{12}\approx\lambda'_{12}\approx 0.6$ and $\lambda_{11}\approx\lambda'_{11}\approx 0.3$, the mass limit is $M_r\gtrsim$180 TeV. A more judicious choice of couplings would relax the mass limit: by tuning the couplings while keeping $\lambda_{11}\lesssim 2$, the limit becomes $M_r\gtrsim$100 TeV.

The scalar leptoquark r has chirality violating couplings since it couples to both left- and right-handed quarks and leptons. It may contribute, at tree level, to decays that are helicity suppressed in the standard model, such as the decays of the pseudoscalar mesons, but without the mass suppression. The new contribution to the decay amplitude interferes with the standard model amplitude, so the leptoquark contribution to the rate scales as $1/M_r^2$. The ratio of the helicity suppressed decay of the pion to the dominant mode is measured to be [1]

$$R\equiv\frac{\Gamma\left(\pi^+\to e^+\nu\right)}{\Gamma\left(\pi^+\to\mu^+\nu\right)}=(1.230\pm 0.004)\times 10^{-4}, \tag{5.5}$$

and the SM prediction is [18] $R_{SM}=(1.2352\pm 0.0001)\times 10^{-4}$. The contribution from exchange of an r leptoquark is

$$\frac{R_{LQ}}{R_{SM}}=\frac{1}{2\sqrt{2}G_F V_{ud}}\frac{m_\pi^2}{m_u+m_d}\frac{1}{M_r^2}\left(\frac{\lambda_{11}\lambda'_{11}}{m_e}-\frac{\lambda_{12}\lambda'_{12}}{m_\mu}\right). \tag{5.6}$$

Since the leptoquark enhances R, and the standard model prediction is already above the observed value, the constraint on the leptoquark is strong. At the 95% CL,

$$\frac{M_r}{\sqrt{\lambda_{11}\lambda'_{11}}}>270\,\text{TeV}. \tag{5.7}$$

As discussed above, $\lambda_{11}\lambda'_{11}\gtrsim 0.1$ so that the pion decays require $M_r\gtrsim 90$ TeV.

At 1-loop the leptoquark contributes to processes like $K-\overline{K}$ mixing or $\mu\to e\gamma$. Let us briefly discuss the former. The contribution to $K_L^0-K_S^0$ mass splitting, Δm_K, from

box diagrams involving r is

$$\Delta m_K^{(LQ)} = \frac{\left(\lambda'_{12}\lambda'_{22}\right)^2}{M_r^2}\frac{f_K^2\, m_K}{192\pi^2}\ , \tag{5.8}$$

where $f_K \approx 159.8\,\text{MeV}$ is the kaon decay constant, and the measured mass splitting is $\Delta m_K = (3.483 \pm 0.006) \times 10^{-12}\,\text{MeV}$. Since there are large long distance uncertainties in the calculation of the SM contribution to Δm_K we will assume that the new physics contribution from r boxes can be as large as 30% of the measured value. Using the values $\lambda'_{12} \approx 0.6$ and $\lambda'_{22} \approx 1.5$, as suggested in section 2, this results in a bound of $M_r \gtrsim 70$ TeV.

Additional constraints on r are set by lepton-flavor violating K decays (such as $K^+ \to \pi^+\,\mu^+\,e^-$), rare τ decays, $D - \overline{D}$, $B_s - \overline{B_s}$ mixing, and other processes. However, the limit on M_r coming from $\mu \to e$ conversion in nuclei is currently the most stringent one. Thus, an improvement in the experimental sensitivity on $\mu \to e$ conversion in nuclei may lead to the discovery of the r leptoquark effects.

The constraints on the fields used to generate the b quark mass, Φ_8 and Φ'_8, are more model dependent. Color-octet weak-doublet scalars of this type have been discussed in Ref. [20, 21]. In our case the flavor structure of their interactions is different, predominately involving a 3rd generation left-handed quark and a right-handed quark of any generation. Through the down-type quark mixing (4.20), Φ'_8 gives tree-level contributions to $K - \overline{K}$ mixing, and together Φ_8 and Φ'_8 give loop contributions to $b \to s\gamma$. Due to the number of small mixings that enter, the constraint from $K - \overline{K}$ mixing is very weak, $M_{8'} \gtrsim \mathcal{O}(10\,\text{GeV})$. The $b \to s\gamma$ process involves fewer mixing insertions and has a stronger constraint. The contribution of Φ_8 is similar to that of a charged Higgs boson. However, because the b quark mass itself is generated at 1 loop, $b \to s\gamma$ is not loop suppressed, but is suppressed by small model-dependent mixings. Depending on these couplings, the Φ_8 mass may be below the TeV scale, making it accessible at the LHC. The color-octet scalar Φ_8 would then be produced in pairs via its coupling to the gluon, and the signal would be a pair of equal mass resonances, such as $(t\,\bar{t})\,(t\,\bar{t})$, $(t\,\bar{b})\,(b\,\bar{t})$, $(j\,\bar{b})\,(b\,j)$, or $(b\,\bar{t})\,(j\,\bar{b})$, where j is a jet coming from an up or charm quark. Some of these signatures have been studied in Ref. [22, 21]. Single Φ_8 production is also possible via gluon fusion [23]. The Φ_8 can also alter the decays of the top quark.

The vectorlike leptons $\Upsilon^{1,2}$ are harder to produce, but their decays (into a charged lepton and two jets via a virtual r at tree level, or into $\tau\gamma$ at 1-loop) are easier to observe.

6 Conclusions

The repeated mass hierarchies amongst elementary fermions is a long-standing mystery in particle physics. We have proposed that the fermion masses are generated by loops involving other standard model fermions. Starting with only the top-quark being heavy at tree level, and introducing a single scalar (leptoquark) which couples the up-type quarks to the leptons, we have shown that all these fermions acquire mass in turn, each at a higher loop level than the previous one. The outcome of this *domino mechanism* is that the τ, c, μ, u and e masses are generated at 1, 2, 3, 4 and 5 loops, respectively. Unlike many other methods for generating the Yukawa couplings, we do not distinguish between the generations of standard fermions. Even the top quark need not be singled out by a symmetry: in the presence of a heavy vectorlike quark, the tree-level mass matrix of the up-type quarks has rank one, such that only the top gets a tree-level mass.

The mechanism may be extended to the down-type quarks by including some other 'domino' particles. The model building aspects here involve more moving parts. We have described an explicit example where the bottom-quark mass is generated by a loop involving a pair of color-octet scalars and the top quark. A byproduct of these color octets is that the charm mass receives additional 2-loop contributions, and the electron mass is generated at 4 loops. The strange- and down-quark masses arise through loops involving the scalar octets and a vectorlike lepton. Altogether, this model induces bottom and tau masses at 1 loop, a charm mass at 2 loops, muon and strange masses at 3 loops, and masses for the first generation at 4 loops. With all couplings of order unity, this generates the correct patterns of fermion masses and CKM matrix elements.

Our mechanism works equally well anywhere between the electroweak and Planck scales. There are however constraints on the masses of the new scalars from various flavor-changing processes. The leptoquark has to be heavier than about 100 TeV, and its effects may be discovered in future experiments searching for $\mu \to e$ conversion in nuclei, or rare K decays. The constraints on the color octets are far weaker, allowing for interesting signatures involving third-generation quarks at the LHC.

Given the relatively high mass required for the leptoquark, our domino mechanism must be embedded in a larger theory that also addresses the stability of the electroweak scale. We expect that it is possible to construct a supersymmetric theory of this type[3]. Another possibility is that the Higgs doublet is a bound state of the top quark with a vec-

[3]Related supersymmetric models can be found in Ref. [24].

torlike quark, as in the top seesaw model [12]. The discovery at colliders of superpartners or of particles involved in dynamical electroweak symmetry breaking could allow tests of the flavor effects induced by the domino particles.

In total there are 24 parameters of our model that are involved in generating the entries of the fermion mass matrices. Once the top mass is fixed, there are only predictions for 8 fermion masses and 4 CKM elements leaving many parameters free. It would be interesting to embed the domino mechanism into a grand unified theory, which would reduce sufficiently the number of parameters to allow definite comparisons with the experimental values. Intriguingly, all scalars introduced in this paper fit into the $\overline{126}$ representation of $SO(10)$.

Acknowledgments: We would like to thank Thomas Becher, Sekhar Chivukula, André de Gouvêa, Ayres Freitas, Dave Kaplan, Andreas Kronfeld, Zoltan Ligeti, Michael Ramsey-Musolf, Chris Quigg, Scott Thomas and Koichi Yamawaki for useful comments. P.J.F. would like to thank the KITP for hospitality while part of this work was completed. This research was supported in part by the National Science Foundation under Grant No. PHY05-51164. B.D. acknowledges the hospitality and support of the Radcliffe Institute for Advanced Study during early stages of this work. Fermilab is operated by Fermi Research Alliance, LLC, under Contract DE-AC02-07CH11359 with the United States Department of Energy.

Appendix: 2-loop integrals

In this Appendix we compute the 2-loop integrals that contribute to the charm mass. Let us begin with the rainbow diagram of Fig. 3:

$$\begin{aligned} \epsilon_r^{(2)} &= N_c \int \frac{d^4k'}{(2\pi)^4} \frac{M_\Psi^2}{k'^2(k'^2 - M_r^2)} \int \frac{d^4k}{(2\pi)^4} \frac{1}{k^2(k^2 - M_\Psi^2)\left[(k-k')^2 - M_r^2\right]} \\ &= \frac{N_c}{(16\pi^2)^2} \int_0^1 dx\, f\left(x, M_\Psi^2/M_r^2\right) \end{aligned} \tag{A.1}$$

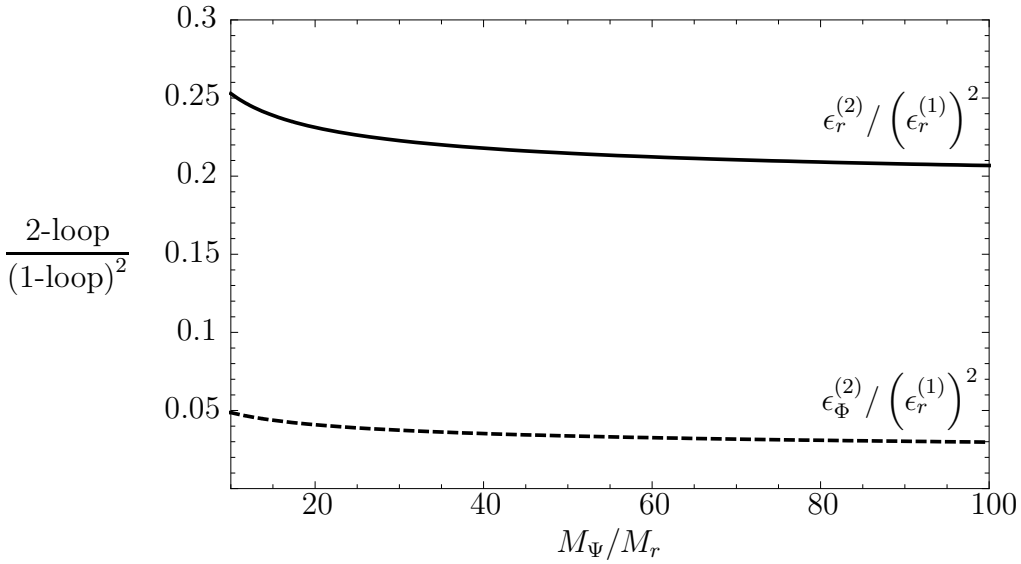

Figure 14: $\epsilon_r^{(2)}$ is the 2-loop factor generated by the rainbow diagram contribution to m_c of Figure 3 and $\epsilon_\Phi^{(2)}$ is from the 2-loop diagram of Figure 9. Here they are plotted relative to the 1-loop contribution to m_τ from Figure 2.

where we defined

$$\begin{aligned} f(x,\,a) &= a\int_{1/[a\,x(1-x)]}^{1/(a\,x)} dt\;\frac{\ln t}{1-t} \\ &= a\left[\mathrm{Li}_2\left(1-\frac{1}{a\,x}\right)-\mathrm{Li}_2\left(1-\frac{1}{a\,x(1-x)}\right)\right]\;. \end{aligned} \tag{A.2}$$

For $M_\Psi^2/M_r^2 \gg 1$,

$$\epsilon_r^{(2)} \approx \frac{N_c}{(16\pi^2)^2}\;\left[\frac{1}{2}\ln^2\left(\frac{M_\Psi^2}{M_r^2}\right)+\ln\left(\frac{M_\Psi^2}{M_r^2}\right)+\frac{391}{400}\right]\;. \tag{A.3}$$

Let us now turn to the 2-loop diagram shown in Fig. 9. The associated 2-loop integral, which contributes to the charm mass as in Eq. (4.6), is

$$\begin{aligned} \epsilon_\Phi^{(2)} &= N_c\int\frac{d^4k'}{(2\pi)^4}\,\frac{M_\Psi^2\,\not{k}'}{k'^2(k'^2-M_8^2)(k'^2-M_\Psi^2)}\int\frac{d^4k}{(2\pi)^4}\,\frac{\not{k}}{k^2(k^2-M_r^2)\,[(k-k')^2-M_r^2]} \\ &= N_c\frac{M_\Psi^2}{16\pi^2}\int_0^1 dx\int_0^1 dy\;\widetilde{I}_1\left(M_\Psi, M_8, M_r\sqrt{(1/x-y)/(1-x)}\right)\;, \end{aligned} \tag{A.4}$$

where $\widetilde{I}_1$ is the 1-loop integral given in Eq. (4.4). For $M_8 \ll M_r, M_\Psi$,

$$\epsilon_\Phi^{(2)} \approx \frac{N_c}{(16\pi^2)^2}\int_0^1 dx\;(1-x)\,f\big(x, M_\Psi^2/M_r^2\big)\;. \tag{A.5}$$

For $M_\Psi^2/M_r^2 \gg 1$,

$$\epsilon_\Phi^{(2)} \approx \frac{N_c}{(16\pi^2)^2}\left[\ln\left(\frac{M_\Psi^2}{M_r^2}\right) - \frac{\pi^2}{6}\right] \ . \tag{A.6}$$

Both $\epsilon_r^{(2)}$ and $\epsilon_\Phi^{(2)}$ are shown in Figure 14.

References

[1] W. M. Yao *et al.* [Particle Data Group], "Review of particle physics," J. Phys. G **33** (2006) 1, and 2007 partial update for the 2008 edition.

[2] For some brief reviews and lists of references, see:
K. S. Babu and E. Ma, "Radiative Mechanisms For Generating Quark And Lepton Masses: Some Recent Developments", Mod. Phys. Lett. A **4**, 1975 (1989);
S. M. Barr, "Radiative Fermion Mass Hierarchy in a Non-supersymmetric Unified Theory," Phys. Rev. D **76**, 105024 (2007) [arXiv:0706.1490 [hep-ph]];
L. E. Ibanez, "Radiative Fermion Masses In Grand Unified Theories," Nucl. Phys. B **193**, 317 (1981);
B. A. Dobrescu, "Fermion masses without Higgs: A Supersymmetric technicolor model," Nucl. Phys. B **449**, 462 (1995) [arXiv:hep-ph/9504399];
T. Appelquist, Y. Bai and M. Piai, "Quark mass ratios and mixing angles from SU(3) family gauge symmetry," Phys. Lett. B **637**, 245 (2006) [arXiv:hep-ph/0603104].

[3] H. Georgi and S. L. Glashow, "Attempts to calculate the electron mass," Phys. Rev. D **7**, 2457 (1973); "Spontaneously broken gauge symmetry and elementary particle masses," Phys. Rev. D **6**, 2977 (1972).
S. Weinberg, "Electromagnetic and weak masses," Phys. Rev. Lett. **29**, 388 (1972).

[4] B. S. Balakrishna, "Fermion Mass Hierarchy From Radiative Corrections," Phys. Rev. Lett. **60**, 1602 (1988);
B. S. Balakrishna, A. L. Kagan and R. N. Mohapatra, "Quark Mixings And Mass Hierarchy From Radiative Corrections", Phys. Lett. B **205**, 345 (1988).

[5] B. S. Balakrishna, "Radiatively Induced Lepton Masses", Phys. Lett. B **214**, 267 (1988).

[6] B. S. Balakrishna and R. N. Mohapatra, "Radiative fermion masses from new physics at TeV scale", Phys. Lett. B **216**, 349 (1989).

[7] Z. z. Xing, H. Zhang and S. Zhou, "Updated Values of Running Quark and Lepton Masses," arXiv:0712.1419 [hep-ph].

[8] S. M. Barr, "An SO(10) Model Of Fermion Masses," Phys. Rev. D **24**, 1895 (1981); L. Ferretti, S. F. King and A. Romanino, "Flavour from accidental symmetries," JHEP **0611**, 078 (2006) [arXiv:hep-ph/0609047].

[9] K. S. Babu and R. N. Mohapatra, " Permutation Symmetry And The Origin Of Fermion Mass Hierarchy", Phys. Rev. Lett. **64**, 2747 (1990).

[10] V. A. Miransky, M. Tanabashi and K. Yamawaki, "Dynamical Electroweak Symmetry Breaking with Large Anomalous Dimension and t Quark Condensate," Phys. Lett. B **221**, 177 (1989); "Is the t Quark Responsible for the Mass of W and Z Bosons?," Mod. Phys. Lett. A **4**, 1043 (1989).

[11] W. A. Bardeen, C. T. Hill and M. Lindner, "Minimal Dynamical Symmetry Breaking Of The Standard Model," Phys. Rev. D **41**, 1647 (1990).

[12] B. A. Dobrescu and C. T. Hill, "Electroweak symmetry breaking via top condensation seesaw," Phys. Rev. Lett. **81**, 2634 (1998) [arXiv:hep-ph/9712319].
R. S. Chivukula, B. A. Dobrescu, H. Georgi and C. T. Hill, "Top quark seesaw theory of electroweak symmetry breaking," Phys. Rev. D **59**, 075003 (1999) [arXiv:hep-ph/9809470].
H. J. He, C. T. Hill and T. M. P. Tait, "Top quark seesaw, vacuum structure and electroweak precision constraints," Phys. Rev. D **65**, 055006 (2002) [arXiv:hep-ph/0108041].

[13] X. G. He, R. R. Volkas and D. D. Wu, "Radiative Generation Of Quark And Lepton Mass Hierarchies From A Top Quark Mass Seed", Phys. Rev. D **41**, 1630 (1990).

[14] K. S. Babu and R. N. Mohapatra, "Top Quark Mass In A Dynamical Symmetry Breaking Scheme With Radiative B Quark And Tau Lepton Masses," Phys. Rev. Lett. **66**, 556 (1991).

[15] R. Rattazzi, "Radiative quark masses constrained by the gauge group only," Z. Phys. C **52**, 575 (1991).

[16] L. Wolfenstein, "Parametrization Of The Kobayashi-Maskawa Matrix," Phys. Rev. Lett. **51**, 1945 (1983).

[17] S. Davidson, D. C. Bailey and B. A. Campbell, "Model independent constraints on leptoquarks from rare processes," Z. Phys. C **61**, 613 (1994) [arXiv:hep-ph/9309310].

[18] V. Cirigliano and I. Rosell, "The Standard Model prediction for $R_{e/mu}^{(pi,K)}$," arXiv:0707.3439 [hep-ph].

[19] R. Kitano, M. Koike and Y. Okada, "Detailed calculation of lepton flavor violating muon electron conversion rate for various nuclei," Phys. Rev. D **66**, 096002 (2002) [Erratum-ibid. D **76**, 059902 (2007)] [arXiv:hep-ph/0203110].

[20] A. V. Manohar and M. B. Wise, "Flavor changing neutral currents, an extended scalar sector, and the Higgs production rate at the LHC," Phys. Rev. D **74**, 035009 (2006) [arXiv:hep-ph/0606172].

[21] M. Gerbush, T. J. Khoo, D. J. Phalen, A. Pierce and D. Tucker-Smith, "Color-octet scalars at the LHC," arXiv:0710.3133 [hep-ph].

[22] B. A. Dobrescu, K. Kong and R. Mahbubani, "Massive color-octet bosons and pairs of resonances at hadron colliders," arXiv:0709.2378 [hep-ph].

[23] M. I. Gresham and M. B. Wise, "Color Octet Scalar Production at the LHC," Phys. Rev. D **76**, 075003 (2007) [arXiv:0706.0909 [hep-ph]].

[24] K. S. Babu, B. S. Balakrishna and R. N. Mohapatra, "Supersymmetric model for fermion mass hierarchy", Phys. Lett. B **237**, 221 (1990);
S. Nandi and Z. Tavartkiladze, "A New Extensions of MSSM: FMSSM," arXiv:0804.1996 [hep-ph].